



Effect of N₂ flow rate on electromagnetic interference shielding effectiveness of TiN_x films

Linlin Lu¹ · Fa Luo¹ · Yuchang Qing¹ · Wancheng Zhou¹ · Dongmei Zhu¹ · Jie Dong¹

Received: 12 June 2018 / Accepted: 25 September 2018 / Published online: 28 September 2018
© Springer-Verlag GmbH Germany, part of Springer Nature 2018

Abstract

TiN_x films with different nitrogen contents were fabricated using direct current reactive magnetron sputtering. Influence of N₂ flow rate on the resistivity and electromagnetic interference (EMI) shielding effectiveness (SE) of TiN_x films was studied. The EMI SE of TiN_x films was found to be related with the resistivity. With the rise of N₂ flow rate, the resistivity of TiN_x films increased, while the EMI SE decreased. When the N₂ flow rate was 1 sccm, the EMI SE of TiN_x films was over 20 dB with the thickness of 1.47 μm, which was much smaller than the thickness of the presently known EMI-shielding materials. The results indicated that TiN_x films could be applied as ultrathin thickness, lightweight, and design flexibility shielding materials.

1 Introduction

The rapid development of electronic devices generates electromagnetic pollution and electromagnetic interference (EMI), which has harmful influence on the equipment performance as well as the surrounding environment for human health [1–4]. As an effective method, EMI shielding is becoming increasingly important to protect human and environment from the negative effects [5–7]. In general, there are two main mechanisms for EMI shielding [8]. The first mechanism is the reflection caused by an interaction between mobile charge carriers with the electromagnetic fields, resulting in the requirement of electrical conductivity of the shielding materials. The second mechanism is the absorption of EMI radiation due to the electric and/or magnetic dipoles interacting with the electric and magnetic vectors of the EM radiation. Both the reflection and absorption characteristics are related to the electrical conductivity of the shielding materials [4]. Consequently, due to a high value of electrical conductivity, metals and alloys are widely used as EMI shields. However, their shortcomings such as heavy weight, susceptibility to corrosion and poor processability restrict their range of application [9–13]. Considerable research efforts have been made for the development of

novel high-performance EMI-shielding materials with lightweight, low cost, good corrosion resistance, and processability to address the adverse effects of EMI during the past two decades [14–16]. In recent years, compared with traditional metal-shielding materials, electrically conductive polymer composites have drawn much attention for combating EMI interference due to the advantages of lightness and resistance to corrosion [7, 17–23]. However, if EMI-shielding effectiveness of these materials meets the demand for over 20 dB, the thickness in the order of millimeter is required for these materials [1, 9, 20, 24–26]. In practical, EMI-shielding applications such as the aerospace, automobiles, and fast-growing next-generation flexible electronics area, there is a greater demand for ultrathin thickness, lightweight, and design flexibility besides high EMI-shielding performance. As a consequence, it is full of significance to develop various ultrathin, lightweight, and flexible EMI-shielding materials.

As a unique transition metal nitride with free-electron-like behavior, TiN film has been widely used in many industries because of its excellent properties, including exceptional hardness, high thermal stability, and high resistance to wear and corrosion [27–29]. Especially, due to its special electronic structure, TiN film exhibits good electrical conductivity [30]. Furthermore, TiN film can be prepared using physical vapor deposition method at room temperature, which is quite simple and without the geometrical constraints of the shape or size of the object. These outstanding properties of TiN film such as good electrical conductivity, lightweight, low cost, ultrathin thickness, and design flexibility suggest that it may be a good candidate for ultrathin

✉ Linlin Lu
lulinlin-1212@163.com

¹ State Key Laboratory of Solidification Processing, School of Materials Science and Engineering, Northwestern Polytechnical University, Xi'an 710072, China

thickness and design flexibility EMI-shielding materials [31, 32]. However, there are few reports on the potential application of TiN film in EMI shielding.

The present study is focused on exploring the electromagnetic interference shielding effectiveness of TiN_x films, which were deposited on glass substrates using direct current reactive magnetron sputtering technology. A series of TiN_x films with different nitrogen contents were obtained by changing the N₂ flow rate during the deposition, and the influence of N₂ flow rate on the resistivity and EMI-shielding effectiveness of TiN_x film was discussed systematically.

2 Experiments

2.1 Deposition of TiN_x films

A JPG-450-sputtering system was used to deposit TiN_x films onto glass substrates with a 99.995% pure Ti target at room temperature. The vacuum chamber was pumped down to a base pressure of 5.0×10^{-4} Pa. Before the sputtering, the glass substrates were ultrasonically cleaned progressively in deionized water, acetone and ethanol for 15 min, respectively. After achieving the ultimate vacuum, the target was pre-sputtered in Ar gas (99.999% pure) for 15 min to remove the surface titanium oxide layer of the target. Before the deposition, the mixture of Ar and N₂ gases (99.999% pure) was let into the chamber through volume flow meters. The Ar gas flow rate was fixed at 80 sccm, while the N₂ flow rate was varied from 1, 2, 4 to 8 sccm. The target-to-substrate distance was adjusted to 60 mm. The deposition pressure and sputtering power were kept at 0.5 Pa and 100 W during the film deposition. By changing the N₂ flow rate and sputtering time, a series of TiN_x films with different nitrogen contents and the same thickness ($1.5 \pm 0.03 \mu\text{m}$) were obtained.

2.2 Characterization techniques

X-ray diffractometry (Philips X'Pert Diffractometer) was employed to identify the phase composition and crystallinity. The analysis was carried out using Cu-K α radiation at 2θ ranging from 30° to 80° . X-ray photoelectron spectroscopic (XPS) measurements were carried out on (ESCALAB 250Xi) X-ray spectrometry to obtain the chemical composition of the film and the stoichiometric ratio of N/Ti. Composition analysis was performed after the surface of TiN_x films was etched with 3 keV Ar⁺, until the oxygen 1 s peak reached a stable minimum value. The film thickness and surface morphology of the films were characterized by a field-emission scanning electron microscope (ZEISS SUPRA 55). EMI-shielding measurements of TiN_x films were carried out in X-band (8–12.4 GHz) by the Agilent vector network analyzer (E8362B). The measurements were carried out on the

films deposited on the glass substrate. The EMI-shielding measurements were performed on both the bare glass substrate and the substrate coated with TiN_x films. The shielding effectiveness for the bare glass was found to be small, even though the glass part was subtracted from the total shielding effectiveness.

3 Results and discussion

3.1 Phase constituent of the films

Figure 1 shows the XRD patterns of TiN_x films deposited at different N₂ flow rates. Single TiN phase with a face-centered cubic crystal structure is observed according to JCPDS No. 87-0628. No peaks of impurities are observed. A strong and sharp diffraction corresponding to (111) crystal plane of TiN_x films suggests an ordered crystalline structure and the preferred growth direction in (111) of films. The preferred orientation of TiN_x films lies on the minimization of the overall energy which is the sum of the surface energy and strain energy. For TiN film, (200) crystal plane has the lowest surface energy, while (111) crystal plane has the lowest strain energy [33]. According to the previous studies [34, 35], the strain energy of TiN film goes up with the thickness of film rising. When the thickness of TiN film increases to over 1 μm , the strain energy is dominant, and TiN film tends to adopt a (111) preferred orientation to reduce strain energy. Consequently, prepared films exhibit a (111) preferred orientation. As the N₂ flow rate increases, the intensity of the (111) peaks goes down and other peaks are almost indiscernible, suggesting the drop in the crystallinity of

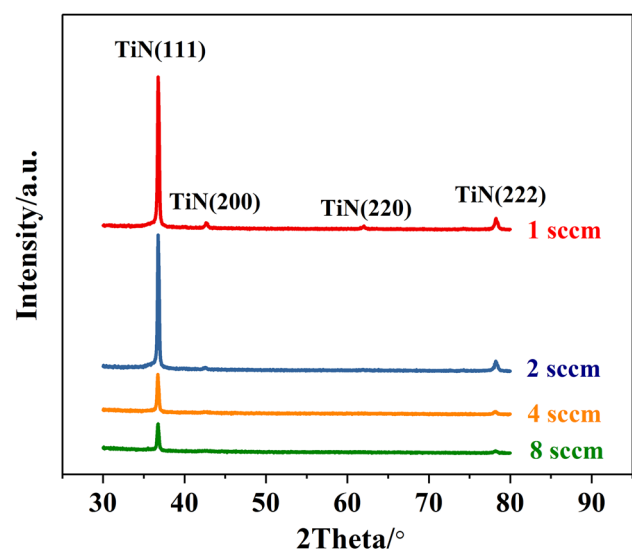


Fig. 1 XRD patterns of TiN_x films at various N₂ flow rates

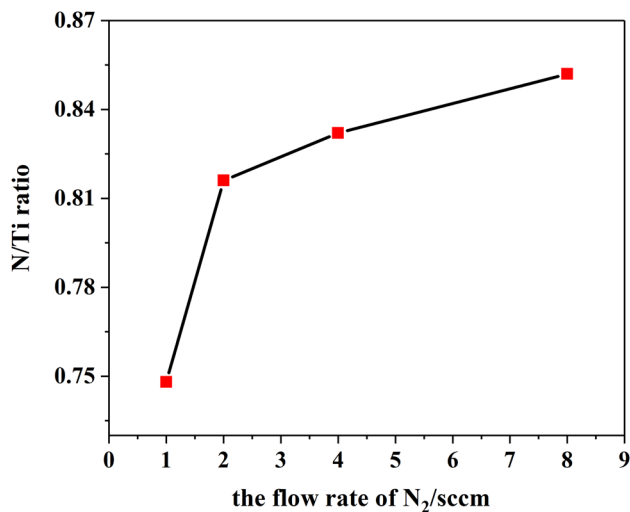


Fig. 2 N/Ti ratio of TiN_x films at various N₂ flow rates

TiN_x films. The collision between Ti and N atoms will become more frequent with the N₂ flow rate rising, leading to a great drop in the energy of atoms. There will be no enough energy for the atoms to fully migrate and rearrange. Therefore, the crystallinity of the film decreases.

To confirm the stoichiometry of TiN_x films, atomic percentage is calculated from the XPS measurements using the appropriate sensitivity factors. As shown in Fig. 2, it reveals an increasing nitrogen content within the films with the N₂ flow rate rising. The N/Ti ratios of TiN_x films increase from 0.74 to 0.85 with the N₂ flow rate rising from 1 to 8 sccm. Based on the Ti–N binary phase diagram, the N/Ti composition range of TiN is 0.6–1.2 [36]. With N₂ flow rate increasing, more and more N atoms collide with Ti atoms, leading to a drop in the relative amount of Ti atoms reaching the substrate. In other words, the number of N atoms reacting with Ti atoms relatively increases, leading to the rise of N/Ti ratio.

Crystallite size (D) of the film can be estimated using the Scherrer formula [37]:

$$D = 0.9\lambda / B \cos\theta, \quad (1)$$

where λ is the wavelength of the incident Cu-K α X-ray (0.1541 nm), B is the full-width at half-maxima (FWHM) of the diffraction peak and θ is the diffraction angle. The result, as shown in Fig. 3, reveals that the crystallite size of the films drops from 40.8 to 33.2 nm with N₂ flow rate rising. The drop of crystallite size is due to the atom collision effects on the kinetic energy. With the N₂ flow rate rising, more frequent collision between Ti and N atoms leads to the decrease in the kinetic energy of the atom. Therefore, there is no enough energy for the depositing atoms to grow up, resulting in smaller crystallite size.

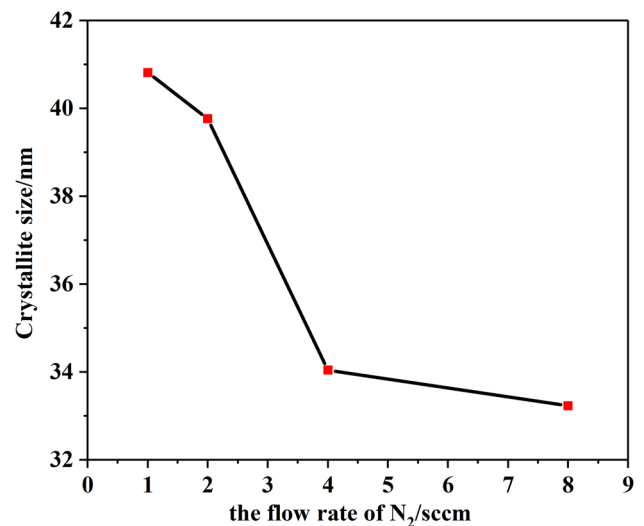


Fig. 3 Crystallite size of TiN_x films at various N₂ flow rates

3.2 Microstructure of the films

Figure 4a–d shows SEM images of TiN_x films at various N₂ flow rates. The SEM images reveal that the nanostructured morphology is dense and uniform with trigonal pyramidal shaped grains on the surface of the films. The thickness of TiN_x films measured using SEM is almost the same (1.5 μ m). According to XRD results, the crystallite size in (111) orientation of TiN_x films decreases with the N₂ flow rate rising. Therefore, the smaller size trigonal pyramidal shaped crystallite will be obtained at the higher N₂ flow rate on the surface of the films.

3.3 Resistivity of TiN_x films

The resistivity of the TiN_x films at different N₂ flow rates is presented in Fig. 5. The resistivity increases from 305 to 673 $\mu\Omega$ cm as N₂ flow rate rises from 1 to 8 sccm. The higher resistivity for higher N₂ flow rate is perhaps contributed to the increment of grain boundary in the film. From the XRD results, it can be known that the grain size drops with N₂ flow rate increasing. Smaller size grain leads to the rise in the number of grain boundaries, and enhances the scattering effect on the free electronic. Moreover, well crystallinity is an important factor to obtain good electrical properties for TiN films, the higher the crystalline degree, the more charge carriers in the film, and thus the better its conductivity is [30].

3.4 EMI-shielding effectiveness of TiN_x films

The EMI-shielding effectiveness of TiN_x films is calculated through the scattering parameters (S parameters)

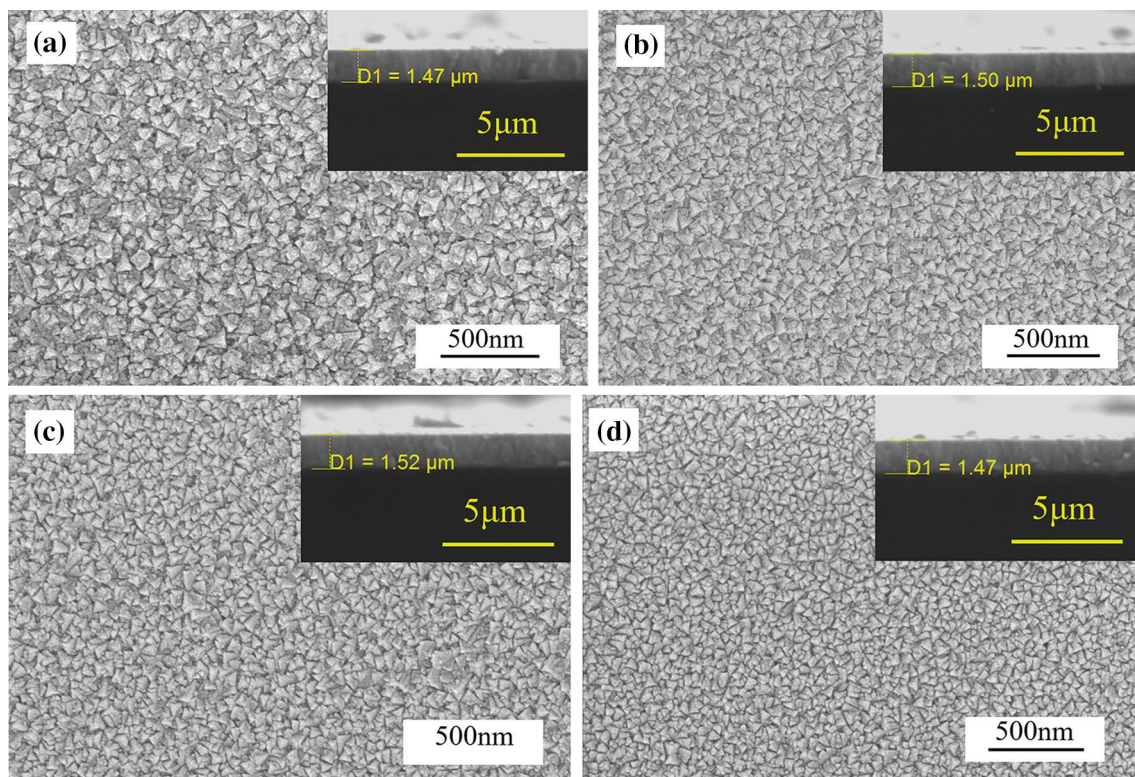


Fig. 4 SEM images of the TiN_x films at various N_2 flow rates **a** 1 sccm, **b** 2 sccm, **c** 4 sccm, and **d** 8 sccm

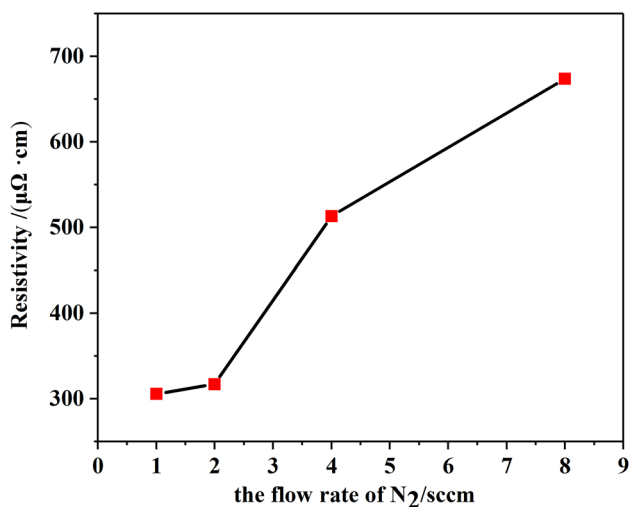


Fig. 5 Resistivity of TiN_x films at various N_2 flow rates

corresponding to the reflection (S_{11}/S_{22}) and transmission (S_{12}/S_{21}) obtained from network analyzer. Shielding effectiveness of glass substrate without films is used as a reference level. The reflectance (R) and transmittance (T) coefficients are evaluated from the scattering parameters using the expressions [20]:

$$R = |S_{11}|^2 = |S_{22}|^2, \quad (2)$$

$$T = |S_{21}|^2 = |S_{12}|^2. \quad (3)$$

The total EMI SE is a combined effort of reflection loss (SE_R), absorption loss (SE_A) and multiple internal reflection (SE_M). At higher EMI SE values (> 15 dB), the SE_M becomes negligible and can be neglected [38]. Therefore, the total SE can be defined as

$$\text{SE}_T = \text{SE}_R + \text{SE}_A. \quad (4)$$

SE_R and SE_A can be expressed in terms of reflection and effective absorption as follows:

$$\text{SE}_R = 10 \times \log \frac{1}{1-R}, \quad (5)$$

$$\text{SE}_A = 10 \times \log \frac{1-R}{T}. \quad (6)$$

Figure 6 shows the comparison of the EMI-shielding effectiveness for glass substrate and films deposited on glass. It is clear that the films show much improved microwave shielding properties comparing to glass substrates. The film deposited at lower N_2 flow rate has a higher value of

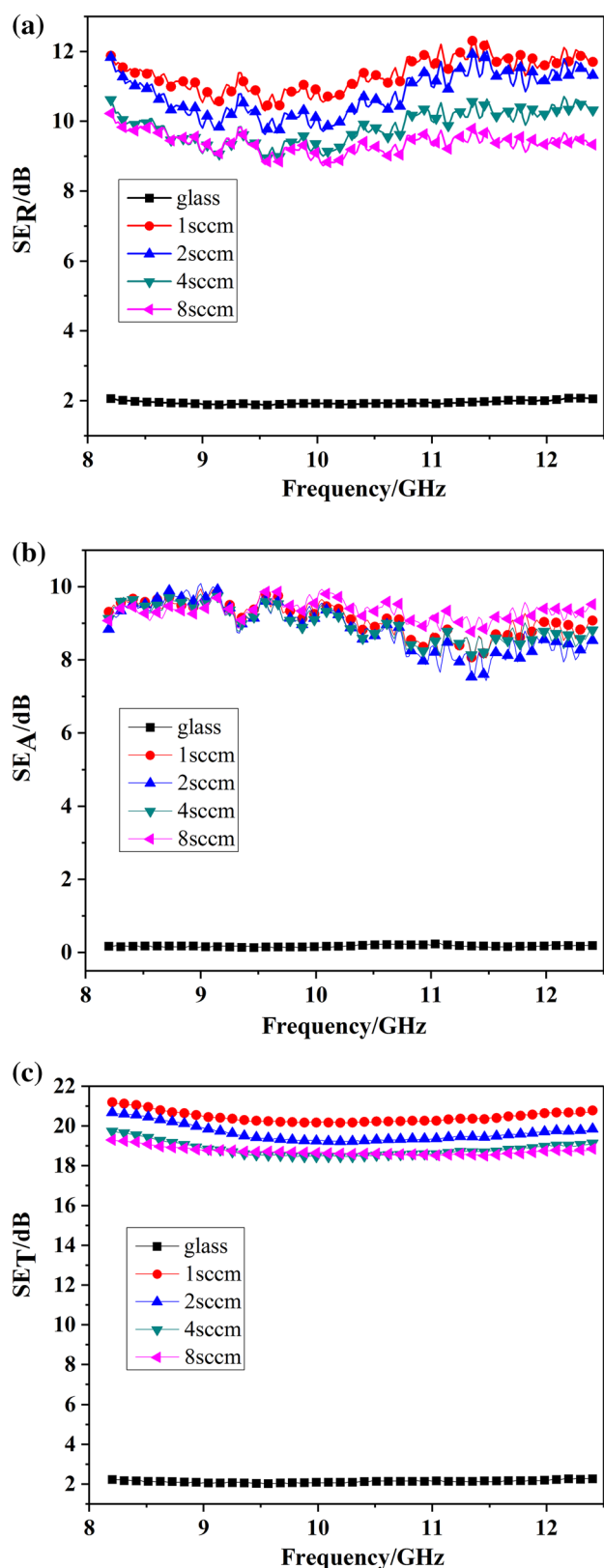


Fig. 6 EMI-shielding effectiveness of the TiN_x films at various N₂ flow rates **a** SE_R, **b** SE_A, **c** SE_T

shielding effectiveness. It can be observed that the shielding effectiveness has a larger value for the reflection as compared to the absorption in the films. Thus, the N₂ flow rate influences the total EMI shielding mainly via the variation in electromagnetic wave reflection performance. The main reason should be ascribed to the increased electrical conductivity. Electrical conductivity is the primary factor to determine EMI-shielding performance, including reflection and absorption of shielding [39]. The SE_R and SE_A are related to the electrical conductivity of composites in the following equations [16]:

$$SE_R = 39.5 + 10\log(\sigma/(2\pi f\mu)), \quad (7)$$

$$SE_A = 8.7d(\pi f\mu\sigma)^{1/2}, \quad (8)$$

where σ , f , μ , and d are the electrical conductivity, the frequency of the electromagnetic wave, the magnetic permeability, and the film thickness, respectively. As shown in equations above, there is a relationship between the SE_R, SE_A, and the electrical conductivity σ of films. A drop in electrical conductivity σ leads to the decrease in SE_R, SE_A, and finally a decrease in SE_T. As noted above, the resistivity of TiN_x films goes up with N₂ flow rate rising, meaning that the electrical conductivity σ drops. Therefore, the SE_R, SE_A, and SE_T values should decrease when N₂ flow rate increases. However, the value of SE_A has little change. The main reason is ascribed to the film thickness d , which is in nanometer scopes and much smaller than the thickness of known EMI-shielding coatings and films [4, 40]. Under the premise of very small thickness, the variation in resistivity causes little change in the value of SE_A based on Eq. (8).

In conclusion, the lower N₂ flow rate is, the high SE_T is. When N₂ flow rate is 1 sccm, the maximum SE_T of TiN_x films is obtained and greater than 20 dB in 8.2–12.4 GHz range. To achieve the similar EMI-shielding value, the thickness of TiN_x films prepared in this work is only 1.47 μm , which is much smaller than the thickness of the presently known EMI-shielding materials. According to the previous reports, to obtain an EMI SE_T of 20 dB in X-band, Yang et al. [41] prepared a carbon nanotube–polystyrene foam composite, and the thickness of composite was about 1.5 mm. Chen et al. [26] fabricated a graphene/PDMS foam composite, and the samples were about 1 mm thick. Maiti et al. [42] developed a lightweight polystyrene/MWCNT/graphite nanoplate nanocomposite, the thickness of samples were 5.6 mm. By contrast, the thickness of TiN_x films in this study is quite small to show remarkable EMI-shielding properties, which may satisfy the requirement of many applications as ultrathin thickness, lightweight, and design flexibility shielding materials [43].

4 Conclusions

TiN_x films with different nitrogen contents were prepared using direct current reactive magnetron sputtering. Influence of N₂ flow rate on the resistivity and electromagnetic interference (EMI) shielding effectiveness (SE) of TiN_x films with the same thickness was studied. With the rise of N₂ flow rate, the resistivity of TiN_x films increased, while the EMI SE decreased. When the flow rate of N₂ was 1 sccm, the EMI SE of TiN_x films was over 20 dB. To achieve the similar EMI-shielding value, the thickness of TiN_x films prepared in this work was only 1.47 μm, which was much smaller than the thickness of the presently known EMI-shielding materials, indicating that the TiN_x films can be applied as ultrathin thickness and design flexibility EMI-shielding materials.

Acknowledgements This work was supported by Fundamental Research Funds for the Central Universities (Grant No. 3102017ZY050), and State Key Laboratory of Solidification Processing (NWP), China (Grant No. KP201604).

References

1. S.T. Hsiao, C.C.M. Ma, H.W. Tien, W.H. Liao, Y.S. Wang, S.M. Li, Y.C. Huang, Using a non-covalent modification to prepare a high electromagnetic interference shielding performance graphene nanosheet/water-borne polyurethane composite. *Carbon* **60**, 57–66 (2013)
2. P.J. Bora, K.J. Vinoy, P.C. Ramamurthy, G. Kishore, Madras, Electromagnetic interference shielding effectiveness of polyaniline-nickel oxide coated cenosphere composite film. *Compos. Commun.* **4**, 37–42 (2017)
3. K. Sabira, M.P. Jayakrishnan, P. Saheeda, S. Jayalekshmi, On the absorption dominated EMI shielding effects in free standing and flexible films of poly (vinylidene fluoride)/graphene nanocomposite. *Eur. Polym. J.* **99**, 437–444 (2018)
4. H.J. Oh, V.D. Dao, H.S. Choi, Electromagnetic shielding effectiveness of a thin silver layer deposited onto PET film via atmospheric pressure plasma reduction. *Appl. Surf. Sci.* **435**, 7–15 (2018)
5. Y. Zhang, Y. Huang, T. Zhang, H. Chang, P. Xiao, H. Chen, Z. Huang, Y. Chen, Broadband and tunable high-performance microwave absorption of an ultralight and highly compressible graphene foam. *Adv. Mater.* **27**, 2049–2053 (2015)
6. Z. Zeng, H. Jin, M. Chen, W. Li, L. Zhou, Z. Zhang, Lightweight and anisotropic porous MWCNT/WPU composites for ultrahigh performance electromagnetic interference shielding. *Adv. Funct. Mater.* **26**, 303–310 (2016)
7. Y. Qing, Y. Mu, Y. Zhou, F. Luo, D. Zhu, W. Zhou, Multiwalled carbon nanotubes–BaTiO₃/silica composites with high complex permittivity and improved electromagnetic interference shielding at elevated temperature. *J. Eur. Ceram. Soc.* **34**, 2229–2237 (2014)
8. S. Frackowiak, J. Ludwiczak, K. Leluk, K. Orzechowski, M. Kozłowski, Foamed poly (lactic acid) composites with carbonaceous fillers for electromagnetic shielding. *Mater. Des.* **65**, 749–756 (2015)
9. H.B. Zhang, W.G. Zheng, Q. Yan, Z.G. Jiang, Z.Z. Yu, The effect of surface chemistry of graphene on rheological and electrical properties of polymethylmethacrylate composites. *Carbon* **50**, 5117–5125 (2012)
10. R. Mohan, S. Varma, M. Faisal, S. Jayalekshmi, Polyaniline/graphene hybrid film as an effective broadband electromagnetic shield. *RSC Adv.* **5**, 5917–5923 (2014)
11. S. Kwon, R. Ma, U. Kim, H.R. Choi, S. Baik, Flexible electromagnetic interference shields made of silver flakes, carbon nanotubes and nitrile butadiene rubber. *Carbon* **68**, 118–124 (2014)
12. R.R. Mohan, S.J. Varma, J. Sankaran, Impressive electromagnetic shielding effects exhibited by highly ordered, micrometer thick polyaniline films. *Appl. Phys. Lett.* **108**, 7–20466 (2016)
13. D.D.L. Chung, Electromagnetic interference shielding effectiveness of carbon materials. *Carbon* **39**, 279–285 (2001)
14. C. Xia, H. Ren, S.Q. Shi, H. Zhang, J. Cheng, L. Cai, K. Chen, H.S. Tan, Natural fiber composites with EMI shielding function fabricated using VARTM and Cu film magnetron sputtering. *Appl. Surf. Sci.* **362**, 335–340 (2016)
15. K. Jagatheesan, A. Ramasamy, A. Das, A. Basu, Electromagnetic shielding behaviour of conductive filler composites and conductive fabrics—a review. *Indian J. Fibre Text.* **39**, 329–342 (2014)
16. G.S. Kumar, D. Vishnupriya, A. Joshi, S. Datar, T.U. Patro, Electromagnetic interference shielding in 1–18 GHz frequency and electrical property correlations in poly (vinylidene fluoride)-multi-walled carbon nanotube composites. *Phys. Chem. Chem. Phys.* **17**, 20347–20360 (2015)
17. S. Hsiao, C. Ma, W. Liao, Y. Wang, S. Li, Y. Huang, R. Yang, W. Liang, Lightweight and flexible reduced graphene oxide/waterborne polyurethane composites with high electrical conductivity and excellent electromagnetic interference shielding performance. *ACS Appl. Mater. Inter.* **6**, 10667–10678 (2014)
18. J.M. Thomassin, C. Jérôme, T. Pardoën, C. Bailly, I. Huynen, C. Detrembleur, Polymer/carbon based composites as electromagnetic interference (EMI) shielding materials. *Mater. Sci. Eng. R* **74**, 211–232 (2013)
19. L.L. Wang, B.K. Tay, K.Y. See, Z. Sun, L.K. Tan, D. Lua, Electromagnetic interference shielding effectiveness of carbon-based materials prepared by screen printing. *Carbon* **47**, 1905–1910 (2009)
20. N. Li, Y. Huang, F. Du, X. He, X. Lin, H. Gao, Y. Ma, F. Li, Y. Chen, P.C. Eklund, Electromagnetic interference (EMI) shielding of single-walled carbon nanotube epoxy composites. *Nano Lett.* **6**, 1141–1145 (2006)
21. V. Eswaraiah, V. Sankaranarayanan, S. Ramaprabhu, Inorganic nanotubes reinforced polyvinylidene fluoride composites as low-cost electromagnetic interference shielding materials. *Nanoscale Res. Lett.* **6**, 137 (2011)
22. V. Eswaraiah, V. Sankaranarayanan, S. Ramaprabhu, Functionalized graphene—PVDF foam composites for EMI shielding. *Macromol. Mater. Eng.* **296**, 894–898 (2011)
23. N. Joseph, M.T. Sebastian, Electromagnetic interference shielding nature of PVDF-carbonyl iron composites. *Mater. Lett.* **90**, 64–67 (2013)
24. Q. Wen, W. Zhou, J. Su, Y. Qing, F. Luo, D. Zhu, High performance electromagnetic interference shielding of lamellar MoSi₂/glass composite coatings by plasma spraying. *J. Alloys Compd.* **666**, 359–365 (2016)
25. A.P. Singh, M. Mishra, D.P. Hashim, T.N. Narayanan, M.G. Hahm, P. Kumar, J. Dwivedi, G. Kedawat, A. Gupta, B.P. Singh, Probing the engineered sandwich network of vertically aligned carbon nanotube—reduced graphene oxide composites for high performance electromagnetic interference shielding applications. *Carbon* **85**, 79–88 (2015)
26. Z. Chen, C. Xu, C. Ma, W. Ren, H.M. Cheng, Lightweight and flexible graphene foam composites for high-performance

- electromagnetic interference shielding. *Adv. Mater.* **25**, 1296–1300 (2013)
27. E. Penilla, J. Wang, Pressure and temperature effects on stoichiometry and microstructure of nitrogen-rich TiN thin films synthesized via reactive magnetron DC-sputtering. *J. Nanomater.* **2008**(5), 145–152 (2014)
 28. W.J. Chou, G.P. Yu, J.H. Huang, Mechanical properties of TiN thin film coatings on 304 stainless steel substrates. *Surf. Coat. Technol.* **149**, 7–13 (2002)
 29. G.L. Zhao, T.B. Zhang, T. Zhang, J.X. Wang, G.R. Han, Electrical and optical properties of titanium nitride coatings prepared by atmospheric pressure chemical vapor deposition. *J. Non-Cryst. Solids* **354**, 1272–1275 (2008)
 30. F. Vaz, J. Ferreira, E. Ribeiro, L. Rebouta, S. Lanceros-Mendez, J.A. Mendes, E. Alves, P. Goudeau, J.P. Riviere, F. Ribeiro, I. Moutinho, K. Pischow, J. de Rijk, Influence of nitrogen content on the structural, mechanical and electrical properties of TiN thin films. *Surf. Coat. Technol.* **191**, 317–323 (2005)
 31. D.Q. Yu, H.P. Xie, L. Wang, Investigation of interfacial microstructure and wetting property of newly developed Sn–Zn–Cu solders with Cu substrate. *J. Alloys Compd.* **385**, 119–125 (2004)
 32. F.Y. Hung, T.S. Lui, H.C. Liao, A study of nano-sized surface coating on LiMn₂O₄ materials. *Appl. Surf. Sci.* **253**, 7443–7448 (2007)
 33. N. Arshi, J.Q. Lu, Y.K. Joo, C.G. Lee, J.H. Yoon, F. Ahmed, Influence of nitrogen gas flow rate on the structural, morphological and electrical properties of sputtered TiN films. *J. Mater. Sci. Mater. Electron.* **24**, 1194–1202 (2013)
 34. H.L. Liang, J. Xu, D.Y. Zhou, X. Sun, S.C. Chu, Y.Z. Bai, Thickness dependent microstructural and electrical properties of TiN thin films prepared by DC reactive magnetron sputtering. *Ceram. Int.* **42**, 2642–2647 (2016)
 35. U.C. Oh, J.H. Je, Effects of strain-energy on the preferred orientation of TiN thin-films. *J. Appl. Phys.* **74**, 1692–1696 (1993)
 36. J.L. Murray, *Phase Diagrams of Binary Titanium Alloys* (ASM International, Ohio, 1987)
 37. B.E. Warren, *X-ray Diffraction*. (Addison Wesley Publishing Co., London, 1969)
 38. X. Li, L. Zhang, X. Yin, L. Feng, Q. Li, Effect of chemical vapor infiltration of SiC on the mechanical and electromagnetic properties of SiN–SiC ceramic. *Scripta Mater.* **63**, 657–660 (2010)
 39. F. Shahzad, M. Alhabeab, C.B. Hatter, B. Anasori, H.S. Man, C.M. Koo, Y. Gogotsi, Electromagnetic interference shielding with 2D transition metal carbides (MXenes). *Science* **353**, 1137–1140 (2016)
 40. X. Zhang, X. Zhang, M. Yang, S. Yang, H. Wu, S. Guo, Y. Wang, Ordered multilayer film of (graphene oxide/polymer and boron nitride/polymer) nanocomposites: an ideal EMI shielding material with excellent electrical insulation and high thermal conductivity. *Compos. Sci. Technol.* **136**, 104–110 (2016)
 41. Y.Y. And, M.C. Gupta, K.L.D. And, R.W. Lawrence, Novel carbon nanotube—polystyrene foam composites for electromagnetic interference shielding. *Nano Lett.* **5**(11), 2131–2134 (2005)
 42. S. Maiti, N.K. Shrivastava, S. Suin, B.B. Khatua, Polystyrene/MWCNT/graphite nanoplate nanocomposites: efficient electromagnetic interference shielding material through graphite nanoplate-MWCNT-graphite nanoplate networking. *ACS Appl. Mater. Inter.* **5**, 4712–4724 (2013)
 43. J. Liang, Y. Wang, Y. Huang, Y. Ma, Z. Liu, J. Cai, C. Zhang, H. Gao, Y. Chen, Electromagnetic interference shielding of graphene/epoxy composites. *Carbon* **47**, 922–925 (2009)